Polypropylene/SiO₂ nanocomposites filled with different nanosilicas: thermal and mechanical properties, morphology and interphase characterization

Rui-Juan Zhou · Thomas Burkhart

Abstract Untreated and surface-treated SiO_2 nanoparticles with different alkyl chain length (described as C0, 3C1, C8 and C16 according to the number of carbon atoms) on particle surface were used as fillers for isotactic polypropylene (iPP). The iPP/SiO_2 composites containing 2.3 vol% of nanoparticles were prepared by melt blending and injection moulding. The dispersion quality of nanoparticles in matrix was examined using scanning electron microscopy (SEM). The crystallization behaviour of iPP was examined using differential scanning calorimetry (DSC). The mechanical properties of all samples were characterized by tensile test, compact tension (CT) test and dynamic mechanical thermal analysis (DMTA). The particle–matrix interphase behaviour was also examined and discussed. SEM images show that different silicas show different dispersion quality in matrix due to different hydrophobicity. The crystallinity and spherulite size of matrix are overall decreased in composites. The tensile properties of iPP/SiO_2 composites show clear relationship with alkyl chain length on particle surface, i.e. increasing alkyl chain length leads to decreased tensile modulus but increased tensile yield strength and strain, indicating increased interfacial interactions with increased alkyl chain length. The 3C1-composite shows the highest fracture toughness with an improvement by 9% compared to neat iPP, whereas the other composites show decreased values of fracture toughness.

R.-J. Zhou (✉) · T. Burkhart
Department of Materials Science, Institute for Composite Materials, Technical University of Kaiserslautern, Erwin-Schrödinger-Str, 67663 Kaiserslautern, Germany
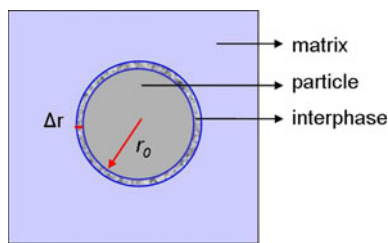e-mail: Ruijuan.zhou@ivw.uni-kl.de

Introduction

Polypropylene (PP) is one of the most widely used polyolefin polymers due to its attractive properties and low cost. It is well known that the mechanical properties of PP can be improved when inorganic fillers are well dispersed in PP matrix [1–6]. One big issue by dispersion of inorganic fillers in PP is the hydrophobic nature of PP itself, which prevents a good interfacial adhesion between hydrophilic fillers and hydrophobic PP matrix. In general, this issue can be overcome by using the following methods: addition of coupling agents such as maleic anhydride-grafted PP, chemical surface treatment of inorganic fillers and in situ polymerization, etc. There are two advantages regarding chemical surface modification of nanoparticles. One is the steric stabilization of nanoparticles towards agglomeration and the other is to improve the compatibility between particle surface and polymer matrix. In the case of nanosilica-filled PP composites, many studies have shown improvements in mechanical properties when silica nanoparticles were chemically surface-treated compared to unmodified silica particles [7–10]. Rong et al. [11, 12] have indicated that a small concentration of modified nanoparticles (nanosilica or nano-$CaCO_3$) less than 3 volume percentage (vol%) can effectively improve the modulus, strength, toughness and thermal deformation temperature of PP.

The mechanical properties of polymer composites depend crucially upon the efficiency of stress transfer from the resin matrix to the fillers, which will be influenced by the interphase. The interphase in composites is the boundary layer between filler surface and polymer matrix, which exhibits local properties different from those of the bulk matrix. In recent years, extensive work has been carried out to correlate the reinforcing ability of composites

Fig. 1 Scheme of interphase between polymer matrix and reinforcing particles

with the strength of the interfacial interactions [13–15]. Unlike fibre-reinforced composites, the interfacial behaviours in particulate-filled polymer composites are difficult to measure directly. Sumita et al. [16] used the energy dissipation in dynamic mechanical analysis (DMA) to identify the effective volume fraction φ_e of dispersed phase as well as the interphase thickness Δr. In this case, the effective volume fraction of dispersed particles composes of the filler volume plus the region of the 'immobilized' matrix associated with the interfaces as described in a simplified mode in Fig. 1. It is thought that the interphase does not contribute to energy dissipation. Accordingly, the ratio of energy dissipated per cycle of vibration in a unit volume for the composite (W_c) to the unfilled system (W_0) is approximately:

$$\frac{W_c}{W_0} = \frac{1}{1 - \varphi_e} \qquad (1)$$

(W_c/W_0) is approximately equal to the ratio of loss modulus (E_c''/E_0''). A parameter B is used to describe the relationship of the effective volume φ_e and the real volume fraction φ_f of the filler. Thus, Eq. 1 can be described as:

$$\frac{W_c}{W_0} = \frac{E_c''}{E_0''} = \frac{1}{1 - \varphi_e} = \frac{1}{1 - \varphi_f \cdot B} \qquad (2)$$

$$B = (1 + \frac{\Delta r}{r})^3 \qquad (3)$$

where r is the radius of a dispersed single nanoparticle.

Rong et al. [15] have used another model developed by Pukánszky and co-workers to predict the interfacial interactions in composites filled with particles:

$$\frac{\sigma_c}{\sigma_0} = \frac{1 - \varphi_f}{1 + 2.5 \cdot \varphi_f} \exp(B_f \cdot \varphi_f) \qquad (4)$$

where σ_c and σ_0 are the yield stresses of the polymer composite and the neat matrix, respectively. B_f is a parameter characterizing the interfacial interactions between matrix and particles.

In this study, isotactic polypropylene (iPP) composites filled with different silica nanoparticles were prepared by direct melt blending. Four commercial nanosilicas were used, in which one was untreated with hydrophilic surface nature after processing; the other three were chemically treated with silanes with different alkyl chain length. It is known that the surface of fumed nanosilicas contains a certain amount of hydroxyl groups (OH) formed during processing due to hydrophilic surface polarity. After chemical treatment with silanes, alkyl chains will be bound via Si–O–SiO$_2$ bridges on particle surface, increasing the hydrophobicity and compatibility of SiO$_2$ nanoparticles in hydrophobic iPP matrix as described in Fig. 2. It is expected that the chemical modification of silica nanoparticles as well as the alkyl chains with different length on particle surface will have an impact on iPP properties. Therefore, the goal of this study was to evaluate the influence of incorporation of nanoparticles, especially the effect of alkyl chain length, on thermal and mechanical properties of iPP. For that purpose, the following properties were characterized and discussed: the hydrophobicity of surface-treated nanoparticles, the dispersion quality of all nanoparticles in iPP matrix, the crystalline behaviour of iPP in respective composites and the mechanical properties of all iPP/SiO$_2$ composites.

Experimental

Materials and sample preparation

Homopolymer iPP granules were purchased from Lyondell Basell Polymers (Moplen-HP 400R). The melt flow rate and the density of this iPP are 25 g/10 min and 0.89 g/cm^3, respectively. The spherical silica nanoparticles were provided from Evonik GmbH, Germany. Their characteristics are given in Table 1. Methanol (99.5%) was purchased from Th. Geyer GmbH, Germany. All materials were used as received.

The iPP granules and all nanoparticles were pre-dried in an oven at 80 °C for 48 h. The nanoparticles were blended with iPP in a Berstorff twin-screw extruder (ZE-25A UTX; KraussMaffei Berstorff GmbH, Germany). The diameter of the screws was 25 mm and the length/diameter ration (L/D) was 44. The process temperature was ranged from 200 °C near the hopper to 220 °C at the die. The screw speed was 150 rpm. Each composite was twice extruded to ensure a better dispersion quality of nanoparticles. After compounding process, the average particle content in respective iPP/SiO$_2$ composites was obtained according to thermogravimetric analysis (TGA, not reported in detail here) as follows: 2.27 vol% for C0–iPP/SiO$_2$, 2.24 vol% for 3C1–iPP/SiO$_2$, 2.26 vol% for C8-iPP/SiO$_2$ and 2.26 vol% for C16-iPP/SiO$_2$. The palletized composite extrudates were then injection moulded into test specimens. Since the particle contents in respective composites are

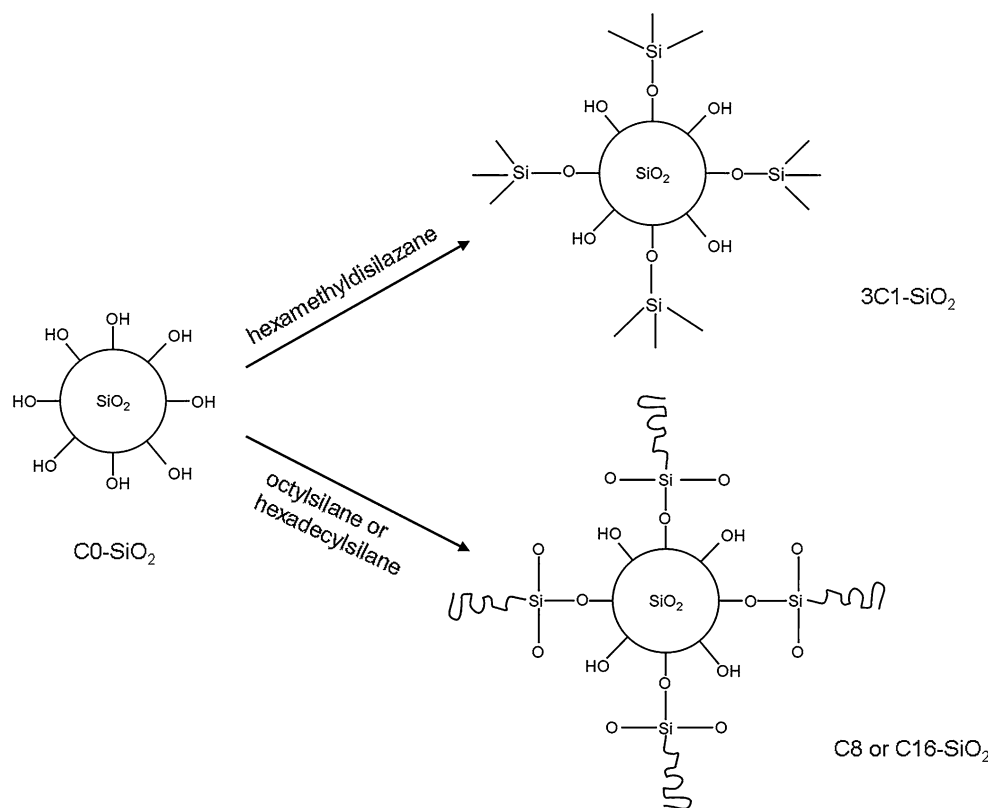**Fig. 2** Chemical structures of untreated and silane-treated silica nanoparticles

Table 1 Important characteristics of SiO$_2$ nanoparticles

Particle types	Specific surface area (m^2/g)	Average diameter (nm)	Carbon content (wt%)	Surface-treated with
Aerosil® 150	150	14	0	Untreated (C0)
Aerosil® R8200	160	12	2.0–4.0	Hexamethyldisilazane (3C1)
Aerosil® R805	150	12	4.5–6.5	Octylsilane (C8)
Aerosil® R816	190	12	0.9–1.8	Hexadecylsilane (C16)

comparable high, an influence of particle content variation on properties of composites is negligible in this study.

Characterization of nanocomposites

Morphology

The dispersion quality of SiO$_2$ nanoparticles in iPP matrix and the morphology of fracture surfaces were examined by using scanning electron microscopy (SEM, JEOL JSM-6300).

The spherulite structure and size of matrix in neat iPP and its composites were also studied using SEM. The samples were etched before SEM examination in an etchant composed of 1 wt% potassium permanganate in a mixture of concentrated sulphuric acid and phosphoric acid in a 3:2 volume ratio. The etch time was 5 h at room

temperature. After etching the samples were cleaned in distilled water and acetone and then dried. All specimens were sputtered with a thin gold film prior to SEM inspection.

Hydrophobicity of nanoparticles

Silica nanoparticles, whose surfaces are modified with non hydrolyzable organic groups, will usually not be wetted by water. However, these nanoparticles can be wetted by a methanol/water mixture. The weight percentage of methanol in this methanol/water mixture is a measure for the hydrophobicity of silica nanoparticles [17]. Accordingly, the relative hydrophobicity of SiO$_2$ nanoparticles used in this work was measured as follows: 200 mg silica nanoparticles and 50 g water were mixed in a 250-mL beaker. If the particles are hydrophobic enough, they will remain on the water surface. Then, methanol (99.5%) was slowly

added into the liquid phase of the mixture using an injection needle. During addition of methanol the mixture in beaker was constantly stirred. A direct contact between the nanoparticles and pure methanol should be avoided. The process was finished when the nanoparticles were totally dispersed in the methanol/water mixture and a relative clear suspension was obtained. The hydrophobicity of respective SiO_2 nanoparticles indicated by methanol-wettability can be calculated as:

$$\frac{m_{\mathrm{m}}}{m_{\mathrm{m}} + m_{\mathrm{H_2O}}} \cdot 100\% \qquad (5)$$

where m_{m} is the amount of methanol used in gram, and $m_{\mathrm{H_2O}}$ is the mass of water (50 g).

Thermal and mechanical properties

Differential scanning calorimetry (DSC) was performed using a Mettler Toledo instrument under nitrogen atmosphere. The following procedure was used: each sample was heated from 50 to 200 °C at a heating rate of 10 °C/min and then held at 200 °C for 5 min to ensure an identical thermal history. The specimen was subsequently cooled down to room temperature at a cooling rate of 10 °C/min.

The dynamic mechanical thermal analysis (DMTA) was carried out using a Gabo Qualimetrer Explexor 25N machine in tension mode. The tests were run in a temperature range of −20 to +140 °C. The frequency and heating rate were 10 Hz and 2 °C/min, respectively. The storage- and loss modulus (E', E''), and the loss factor, tanδ, were obtained.

The tensile test was performed using a Zwick 1474 universal testing machine (Roell, Germany) according to DIN EN ISO 527-2 (dog-bone-shaped specimens) at room temperature. The crosshead speed was 4 mm/min. The tensile modulus was determined by using a clip-on extensometer between 0.05% and 0.25% linear elongation.

Compact tension (CT) examination was performed at room temperature using the same Zwick testing machine at a testing rate of 0.3 mm/min. The samples were prepared according to ASTM D5045-99 and ASTM E399-90 standards ($36 \times 36 \times 4$ mm³). The sharp pre-crack was made by knocking a razor-blade into the samples saw slot. The pre-crack length, a_0, and the ligament length, W, should be prepared in such a way that the condition $0.45 < a_0/W < 0.55$ was satisfied to ensure the plane strain state according to the standards. The specific fracture toughness K_{IC} was calculated as:

$$K_{\mathrm{IC}} = \frac{F_{Q,\mathrm{max}}}{B \cdot \sqrt{W}} \cdot f(a_0/W) \qquad (6)$$

where $f(a_0/W)$ is a tabulated correction function according to ISO 13586, B, W and a_0 are specimen dimensions

(thickness, ligament length and pre-crack length, respectively), $F_{Q,\mathrm{max}}$ is the maximum force in the force–displacement curve.

At least five specimens were tested for DSC, DMTA, tensile and CT-tests. Finally, the average values were taken and represented in this study.

Results and discussion

Dispersion and hydrophobicity of nanoparticles

Figure 3 shows SEM micrographs of respective iPP/SiO₂ nanocomposites. It is clear that the 3C1–SiO₂ and C8–SiO₂ are well dispersed in iPP matrix. Conversely, the untreated and C16–SiO₂ particles form more agglomerates and particle clusters as marked in the images. It is well known that the hydroxyl groups on particle surface can build up hydrogen bonds amongst particles, leading to higher degree of agglomeration. This should be the reason for agglomerated C0–SiO₂ particles. In the case of surface-modified nanoparticles, the long alkyl chains on particle surface can prevent the formation of hydrogen bonds due to steric hindrance. On the other hand, Bagwe et al. [18] concluded that the silica nanoparticles with long alkyl chains (C18) on the particle surface have a much smaller shear or slippage plane, and the long alkyl chains extending from the particle surface are beyond the shear plane. Hence, such nanoparticles agglomerate easily due to strong hydrophobic interaction amongst nanoparticles. This conclusion may explain the higher degree of agglomeration of C16–SiO₂ nanoparticles in our work.

The hydrophobicity measurements show that the 3C1–SiO₂ reveals the highest hydrophobicity with 63.5% methanol-wettability. The C8-nanoparticles show lower hydrophobicity than 3C1-nanoparticles with 56.2% methanol-wettability. Both silicas could not be wetted in water before addition of methanol. On the contrary, the C16-nanoparticles were totally wetted in pure water like untreated nanoparticles, indicating a very low hydrophobicity. This result should be attributed to different degrees of alkylation of silica nanoparticles indicated by the number of alkyl chains on the particle surface. Based on carbon content in respective silica nanoparticles given in Table 1 and the alkyl chain length, it can be concluded that the degree of alkylation of respective SiO₂ nanoparticles decreases with the following order: 3C1–SiO₂ > C8–SiO₂ > C16–SiO₂. This order correlates well with the results of hydrophobicity measurements. The higher the hydrophobicity of SiO₂ nanoparticles, the better they should be dispersed in hydrophobic iPP matrix. This is in agreement with SEM micrographs discussed above.
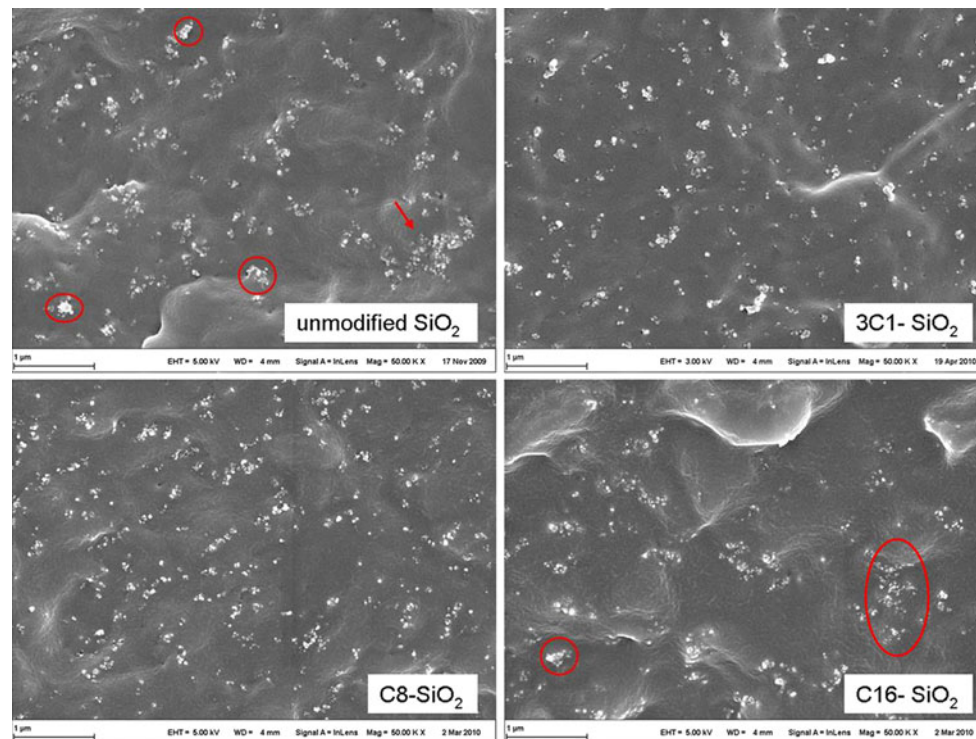
Fig. 3 SEM micrographs of iPP/SiO$_2$ nanocomposites (scale in pictures: 1 μm)

DSC results

The effect of surface-treated and untreated SiO$_2$ nanoparticles on crystallization behaviour of iPP was determined by DSC measurements. The important data obtained are listed in Table 2. From the results, the melting temperatures, T_m, of iPP matrix in all composites are slightly decreased compared to neat iPP. The addition of untreated SiO$_2$ nanoparticles shows no effect on the crystallinity of matrix although the crystallization process starts at a little higher temperature. The crystallinity values of iPP matrix in surface-treated SiO$_2$ filled composites are decreased up to a maximum of 1.9% achieved by C8-composite. The crystalline temperatures of iPP in 3C1-, C8- and C16-composites are slightly increased with a maximum improvement of 1.1 °C. Based on these results, it can be concluded that the crystalline features of iPP have not been

influenced greatly by addition of both treated and untreated silica nanoparticles. This result is in good agreement with previous studies [12, 19]. The SEM micrographs in Fig. 4 show spherulite features of matrix in neat iPP and iPP/SiO$_2$ composites. It can be seen that the neat iPP shows typical three-dimensional spherulites with clear boundaries. The iPP spherulites are 10–20 μm in diameter. Conversely, no spherulitic structure is observed in all iPP/SiO$_2$ composites. The reason for that should be the presence of nanoparticles preventing the growth of iPP crystals due to small inter-particle distances.

DMTA results and interphase behaviour

It was reported that good dispersion quality and strong interfacial interactions between particles and polymer matrix will restrict the movement of matrix molecules,

Table 2 Effect of surface-treated and untreated silicas on the crystallization behaviour of iPP in composites

Samples	Melt temperature T_m (°C)	Crystalline enthalpy ΔH_m (J/g)	Crystallinity X_c (%)[a]	Crystalline temperature T_c (°C)
Neat iPP	168.4	101.2	48.4	116.0
C0–iPP/SiO$_2$	167.0	101.0	48.3	116.9
3C1–iPP/SiO$_2$	168.2	98.0	46.9	116.2
C8–iPP/SiO$_2$	167.7	97.2	46.5	116.6
C16–iPP/SiO$_2$	167.3	97.6	46.7	117.1

[a] Degree of crystallinity calculated using ΔH of iPP equilibrium crystals 209 J/g [33]
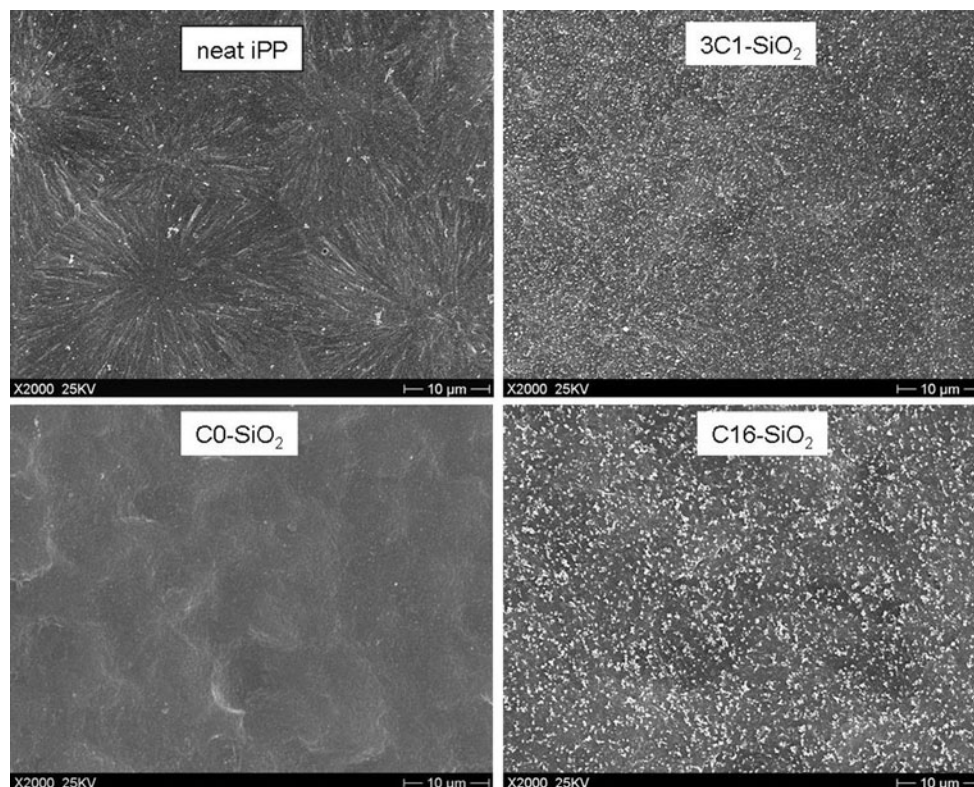
Fig. 4 Spherulite structure and size in neat iPP and iPP/SiO$_2$ composites

resulting in an increase of glass transition temperature (T_g) [15]. Figure 5 shows the mechanical loss factor, tanδ, as a function of temperature for all samples, because tanδ is a sensitive indicator of molecular motions and phase transition. It can be seen that the tanδ curves of all samples exhibit two relaxation peaks within selected temperature range. The first peak around 12 °C corresponds to the glass transition of amorphous iPP (β-relaxation). Evidently, the 3C1–iPP/SiO$_2$ composite shows the highest intensity of β-transition peak amongst all samples, and this β-peak is clearly shifted to higher temperature compared to neat iPP. The C8–iPP/SiO$_2$ and C16–iPP/SiO$_2$ composites show comparable β-peak intensity as neat matrix, whereas the composite filled with untreated SiO$_2$ nanoparticles shows clearly decreased β-peak intensity compared to iPP matrix. This is related to increased interfacial interactions between iPP matrix and silane-treated SiO$_2$ nanoparticles. The second transition peak around 110 °C in Fig. 5 is attributed to α-transition of crystalline iPP due to crystal–crystal slippage motion [20]. The broadness of this peak may indicate a distribution of lamellar thickness of iPP crystals. The storage- and loss modulus (E', E'') at 23 °C, and the β-transition temperature T_β of all samples are summarized in Table 3. From the results, the incorporation of all silica nanoparticles in iPP significantly improves the storage- and loss modulus of composites. The β-transition temperatures

of iPP/SiO$_2$ composites are slightly increased compared to neat iPP. The 3C1–iPP/SiO$_2$ composite shows the highest moduli values and the highest β-transition temperature amongst the composites, whereas the C0-composite shows relative high moduli and the lowest T_β value. This DMTA result can be attributed to different dispersion quality of respective nanosilicas and slightly decreased crystallinity of matrix in composites.

Based on Sumita's model, the effective volume fraction of nanoparticles and the interphase thickness in respective nanocomposites can be quantitatively characterized. From the results given in Table 3, the 3C1-composite exhibits the largest effective volume fraction (φ_e) and interphase thickness (Δr) amongst the composites. The largest effective volume fraction can be partly attributed to the perfect dispersion of 3C1–SiO$_2$ nanoparticles and subsequently the largest contact interphase with matrix, because φ_e is the sum of real volume fraction plus interphase regions. The obtained interphase thickness of composites decreases with the following order: 3C1-composite > C0-composite > C8-composite > C16-composite. There is no clear relationship with alkyl chain length. It should be noted that the calculated values using indirect method are not sensitive enough and they suffer from the fact that simplifying assumptions are made in the calculation. Actually, the chemical modification of nanoparticles creates an organic
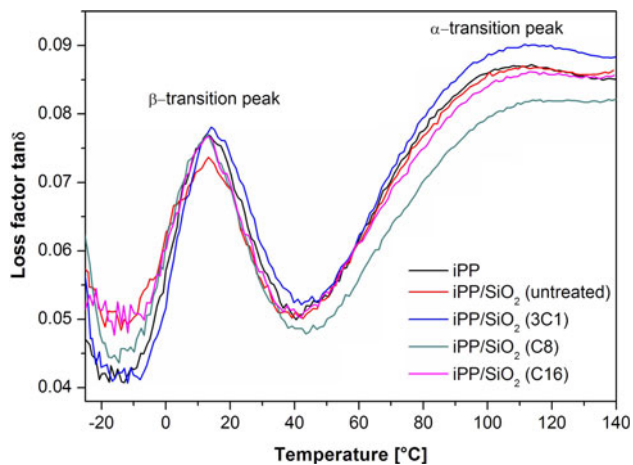
Fig. 5 Mechanical loss factor tanδ as a function of temperature for all samples

coating layer on particle surface which increases the interphase thickness as shown in Fig. 6. According to the simplified model, a hydrophilic–hydrophobic repulsive interaction exists between iPP and untreated SiO$_2$ nanoparticles resulting in an interphase. After surface modification, the introduced alkyl chains stretch far away from the particle surface, interacting with matrix molecules at interface and increasing the thickness of the interphase. Therefore, the interphase thickness in modified SiO$_2$-filled composites should be larger than that in unmodified SiO$_2$-filled composite. However, the interphase thickness for a particle–polymer system is not a constant size because the interphase has no well-defined border with the bulk polymer. On the other hand, the effective interphase thickness depends on many parameters such as chain flexibility, energy of molecular adsorption, the extent of chain entanglements at interface, etc. [21]. Osman and Atallah [19] suggested that the interphase thickness in particulate-filled polymer composites increases with increasing alkyl chain length on particle surface.

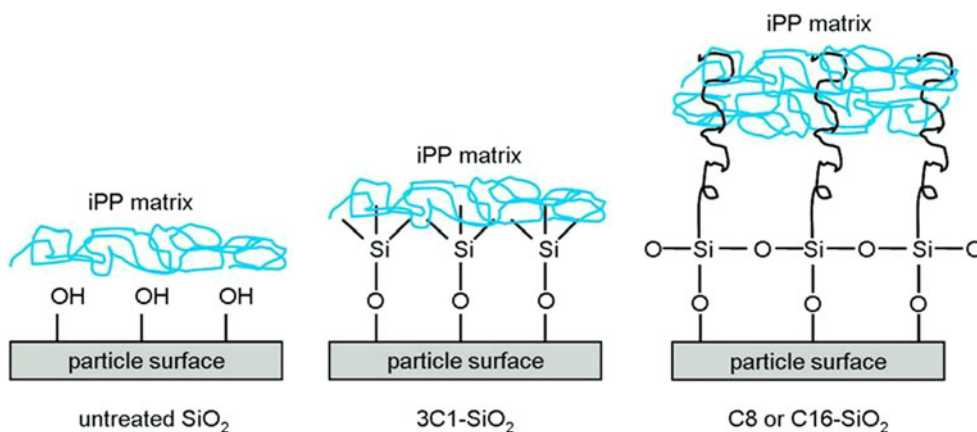Results of tensile measurements and interfacial interactions

The typical stress–strain curves (S–S-curves) of tensile tests for all samples are shown in Fig. 7. From the S–S-curves,

the incorporation of all SiO$_2$ nanoparticles reinforces iPP but reduces the ductility of matrix. The relative improvements in tensile modulus, yield strength and yield strain of iPP/SiO$_2$ nanocomposites based on neat iPP are displayed in Fig. 8a as a function of alkyl chain length. It can be seen that the incorporation of all types of nanoparticles significantly increases the material stiffness indicated by overall increased tensile modulus. Since the crystallinity and spherulite size of matrix in iPP/SiO$_2$ composites are decreased compared to neat iPP, the increase in tensile modulus should be attributed to the rigid particles themselves. The maximum improvement in tensile modulus is 21% achieved by C0–iPP/SiO$_2$ composite. Increasing alkyl chain length leads to clearly decreased tensile modulus. This dropping trend amongst composites can be explained as follows: first, the crystallinity of matrix in composites slightly decreases with increasing alkyl chain length; second, it is reported that the alkyl chains in particle–matrix interphase can act as plasticizers reducing the stiffness of boundary layers, and this effect increases with increasing chain length [22, 23]. Unlike tensile modulus, the yield strength and strain increase with increasing alkyl chain length. Generally, the tensile strength mainly depends on the interfacial interactions between polymer matrix and fillers. In C0–composite, the interfacial adhesion is very poor due to hydrophilic–hydrophobic repulsion force. Therefore, the yield strength of C0-composite is decreased compared to neat iPP. The introduction of alkyl chains on particle surface increases the hydrophobicity of silica particles and leads to increased interfacial interactions due to chain entanglements at interface. As a result, the tensile yield strength also increases. The 3C1-composite exhibits comparable yield strength as neat iPP because the degree of chain entanglements at matrix–particle interface is very low due to short methyl groups. Increasing alkyl chain length on particle surface leads to increased degree of chain entanglements resulting in increased tensile yield strength of C8- and C16-composites. Correspondingly, the interfacial interaction parameter, B_f, calculated according to Eq. 4 shows an increasing tendency with increasing alkyl chain length as shown in Fig. 8b. The dominated influencing factor for tensile strain is usually the interfacial slippage. With increasing alkyl chain length the interfacial slippage

Table 3 DMTA results and interphase parameters obtained according to Eqs. 2 and 3

Samples	φ_f (vol%)	$E'_{23\,°C}$ (MPa)	$E''_{23\,°C}$ (MPa)	T_β (°C)	φ_e (vol%)	Δr (nm)
Neat iPP	–	1762 ± 131	128.4 ± 1.5	12.4	–	–
C0–iPP/SiO$_2$	2.27	2150 ± 122	139.3 ± 1.7	12.8	7.96	3.93
3C1–iPP/SiO$_2$	2.24	2214 ± 71	147.2 ± 1.9	14.9	12.53	5.25
C8-iPP/SiO$_2$	2.26	1955 ± 78	137.5 ± 3.9	13.3	7.07	2.46
C16-iPP/SiO$_2$	2.26	2051 ± 61	136.7 ± 2.0	13.3	5.51	2.03

Fig. 6 Schematic
representation of the interphase
in iPP/SiO$_2$ composites

becomes more difficult due to increased interfacial inter-actions, resulting in higher tensile strain. At a certain degree of deformation, the interfacial slippage between particle surface and polymer matrix leads to debonding of particles.

Compared with iPP/SiO$_2$ nanocomposites filled with polymer-grafted (PS, PMMA, etc.) silica nanoparticles in [15], the iPP/SiO$_2$ nanocomposites in this work show much lower yield strength and B_f values due to much shorter alkyl chains on SiO$_2$ surface. This is also an evidence of increased interfacial interactions with increased chain length in boundary layer.

Results of CT-tests: fracture toughness, mechanisms and morphology

Figure 9a shows the force–displacement curves of all iPP samples. It is evident that the incorporation of C8-, C16- and C0-SiO$_2$ nanoparticles leads to decreased load maxi-mum (F_{max}) at which the initial crack starts to propagate, whereas the 3C1–iPP/SiO$_2$ nanocomposite shows obviously
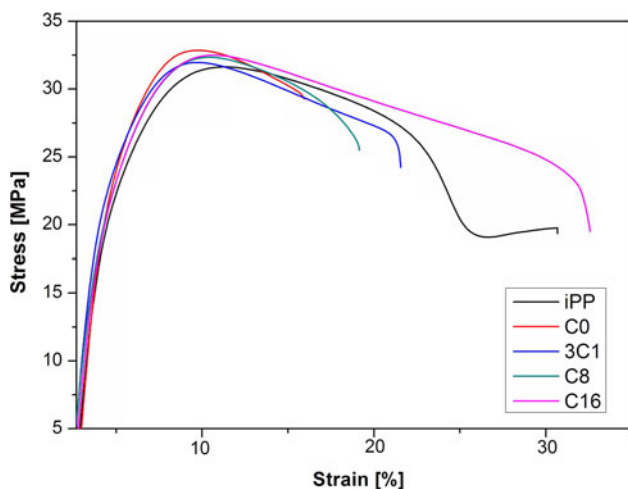

Fig. 7 Stress–strain curves for all samples obtained by tensile tests

increased F_{max} compared to neat iPP. Correspondingly, the fracture toughness K_{IC} obtained from F_{max} decreases with the following order: 3C1–iPP/SiO$_2$ > neat iPP > C0–iPP/SiO$_2$ > C8–iPP/SiO$_2$ > C16–iPP/SiO$_2$ as shown in Fig. 9b. The improvement in fracture toughness of 3C1–iPP/SiO$_2$ composite is about 9%.

It is known that the process of crack propagation and fracture starts with the plastic deformation of the polymer matrix ahead of the initial crack. In particulate-filled polymer nanocomposites, the micromechanisms leading to the plastic deformation are the debonding of particles (creating dimples) and the further plastic flow of the matrix zones, which are locally stretched until rupture by tearing. In general, the failure sequence can be briefly described in two steps as shown in Fig. 10, namely formation of voids (debonding) and subsequent coalescence of voids under imposed load [24]. In iPP/nanoparticle composites, deb-onding is believed to be the initial damage mechanism because of the low polarity and consequently low surface free energy of iPP matrix [25, 26]. Figure 11a shows the morphology of fracture surfaces of iPP and its composites after CT-tests. Macroscopically, neat iPP, C8-composite and 3C1–composite show similar fracture surfaces with increased fracture zone on which macro plastic deforma-tion is observed. Differently, C16-composite and untreated SiO$_2$-filled composite show much longer fracture zones but less plastic deformation on the surfaces, particularly the fracture surface of C16-composite is very smooth. A close examination of the fracture zones near the initial crack tip is shown in Fig. 11b for composites. It can be seen that all composites exhibit numerous dimples and micro plastic deformation on the fracture surfaces. The C0–iPP/SiO$_2$ composite shows the highest degree of micro plastic deformation but the lowest number of dimples. With increasing alkyl chain length, the plastic deformation of matrix decreases whereas the number of dimples increases. At the same volume content of SiO$_2$ nanoparticles, the increase in number of dimples can be attributed to

Fig. 8 **a** Relative improvements in tensile properties of iPP/SiO$_2$ composites containing 2.3 vol% of nanoparticles as a function of alkyl chain length, **b** interfacial interaction parameter, B_f, calculated according to Eq. 4 in different iPP/SiO$_2$ nanocomposites
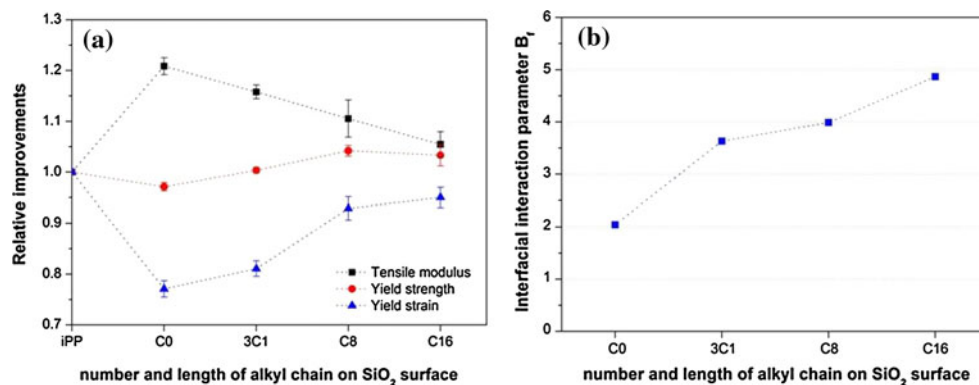

Fig. 9 **a** Load–displacement curves of iPP and its nanocomposites obtained by CT-tests, **b** fracture toughness of all samples as a function of alkyl chain length
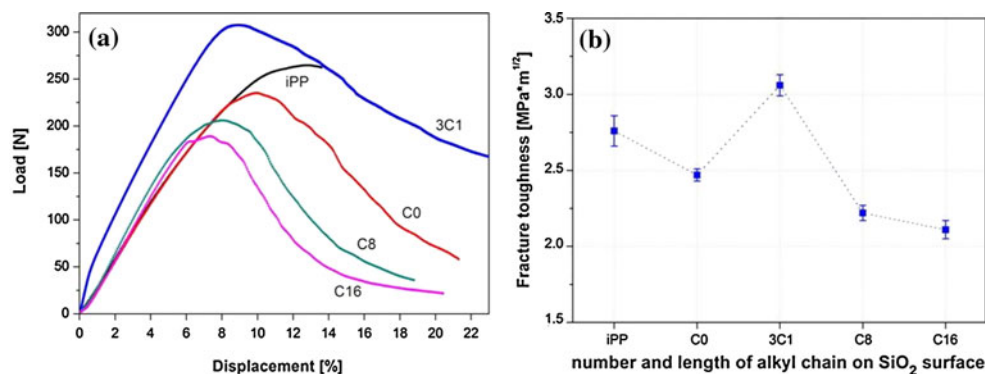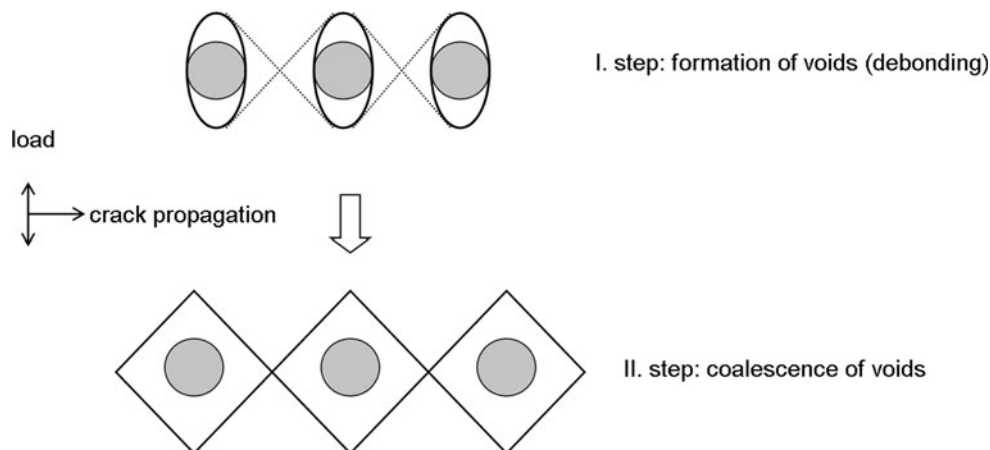

Fig. 10 Formation and coalescence of voids around rigid particles in a ductile polymer matrix under imposed load

increased stress concentration effect of nanoparticles due to increased interfacial interactions. In C0–iPP/SiO$_2$ composite, the nanoparticles and agglomerates detach easily from iPP matrix because of poor matrix–particle adhesion, forming less but larger voids. On one hand, it is believed that the formation of more dimples in fracture process is accompanied by more energy dissipation, leading to higher fracture toughness [27–29]. On the other hand, more voids (dimples) result in smaller matrix zone on the fracture surface. Consequently, the degree of plastic deformation of matrix is reduced by coalescence of voids. This leads finally to easier crack propagation and even ductile–brittle

transition. Obviously, the obtained fracture toughness of iPP/SiO$_2$ nanocomposites is a result of combined positive and negative effects. The 3C1–iPP/SiO$_2$ composite exhibits improved fracture toughness compared to neat iPP, because the positive effect related to the formation of dimples is dominant. In other iPP/SiO$_2$ composites, the negative effect related to less plastic deformation by coalescence of voids is more dominant therefore the values of their fracture toughness are decreased.

Correlating the crystalline behaviour and mechanical properties of iPP/SiO$_2$ composites, one can conclude that the improvements in tensile properties of composites are
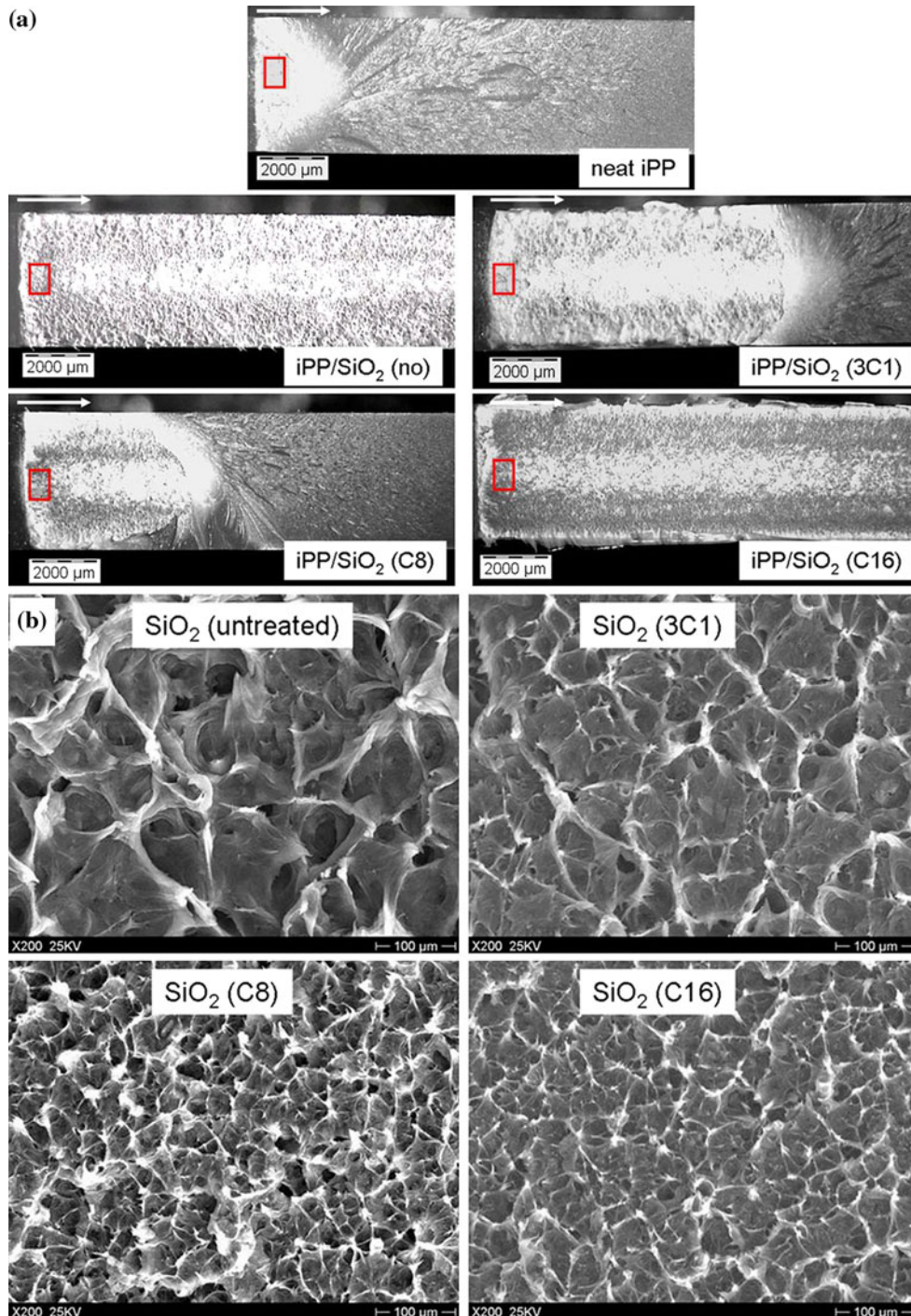
Fig. 11 SEM micrographs of fractured CT-samples: **a** overview of fracture surfaces, **b** close view of the selected fracture zones. The *arrows* in **a** indicate the direction of crack propagation. The *squares* ahead of the pre-cracks indicate the positions where the fracture surfaces in **b** are taken

mainly caused by the change of the stress state around the nanoparticles, because decreased crystallinity and spherulite size can only lead to decreased stiffness and strength [30]. In the case of fracture toughness, Friedrich [31] concluded that the semi-crystalline polymer with smaller spherulites tends to be tougher than the one with larger spherulites. However, Ouederni and Philips [32] found that for a given crystallinity, the reduction of spherulite size via the use of a nucleating agent did not benefit the toughness of PP. Obviously, the effect of crystalline behaviour of matrix on the fracture toughness of a crystalline polymer is very complicated and needs further to be investigated.

Conclusion

In this study, the untreated and silane-treated SiO_2 nanoparticles were compounded in iPP by direct melt blending. The 3C1- and C8–SiO_2 nanoparticles show very good dispersion in iPP matrix due to higher degrees of hydrophobicity. The untreated and C16–SiO_2 nanoparticles agglomerate in some degree because of their lower hydrophobicity. The incorporation of all SiO_2 particles shows little influence on the crystallization behaviour of iPP. However, the spherulite size of iPP in all composites is dramatically decreased compared to neat iPP. From DMTA measurements, both storage modulus and loss modulus of all iPP/SiO_2 nanocomposites are significantly increased. The glass transition temperature of matrix in all composites is slightly increased up to 2.5 °C. The mechanical properties of iPP/SiO_2 composites show a clear relationship with alkyl chain length on particle surface, i.e. the tensile modulus of all composites decreases with increasing alkyl chain length on particle surface. The maximum improvement in tensile modulus is about 21% achieved by C0–iPP/SiO_2 composite. By contrast, the yield strength and strain of composites increase with increasing alkyl chain length. The fracture toughness of most iPP/SiO_2 composites is decreased compared to neat iPP except for 3C1-composite which exhibits an improvement in fracture toughness by 9%.

References

1. Streller RC, Thomann R, Torno O, Mülhaupt R (2008) Macromol Mater Eng 293:218
2. Mittal V (2007) J Thermoplast Compos Mater 20:575
3. Yuan Q, Wu DY, Gotama J, Bateman S (2008) J Thermoplast Compos Mater 21:195
4. Liu XH, Wu QJ (2001) Polymer 42:10013
5. Nejad SJ, Ahmadi SJ, Abolghasemi H, Mohaddespour A (2007) J Appl Sci 7:2480
6. Vu-Khanh T, Fisa B (1986) Polym Compos 7:375
7. Rong MZ, Zhang MQ, Zheng YX, Zeng HM, Freidrich K (2001) Polymer 42:3301
8. Pustak A, Smit I, Svab I, Musil V (2007) Proceedings of conference microscopy-advanced tools for tomorrow's materials, Berlin
9. Garcia M, Van Vliet G, Jain S, Schrauwen BAG, Sarkissov A, Van Zyl WE, Boukamp B (2004) Rev Adv Mater Sci 6:169
10. Huang L, Zhan RB, Lu YF (2009) J Reinf Plast Compos 25:1001
11. Rong MZ, Zhang MQ, Zheng YX, Zeng HM, Walter R, Friedrich K (2000) J Mater Sci Lett 19:1159
12. Rong MZ, Zhang MQ, Zheng YX, Zeng HM, Walter R, Friedrich K (2001) Polymer 42:167
13. Jancar J, Dibenedetto AT, Dianselmo A (1999) Polym Eng Sci 33:559
14. Pukanszky B, Turcsanyi B, Tudos F (1988) In: Ishida H (ed) Interfaces in polymer. Elsevier, New York, p 467
15. Rong MZ, Zhang MQ, Pan SL, Lehmann B, Friedrich K (2004) Polym Int 53:176
16. Sumita M, Tsukihi H, Miyasaka K, Ishikawa K (1984) J Appl Polym Sci 29:1523
17. Oelmüller R, Müller A, Meier K(1997) in Teilhydrophobe Fällungskieselsäuren, identification: DE19713316A1, Degussa AG, Germany
18. Bagwe RP, Hilliard LR, Tan WH (2006) Langmuir 22:4357
19. Osman MA, Atallah A (2007) Macromol Chem Phys 208:87
20. Paul SA, Sinturel C, Joseph K, Gem Mathew GD, Pothan LA, Thomas S (2010) Polym Eng Sci 50:384
21. Ciprari D, Jacob K, Tannenbaum R (2006) Macromolecules 39:6565
22. Rong MZ, Zhang MQ, Pan SL, Friedrich K (2004) J Polym Appl Sci 92:1771
23. Zhou JP, Qiu KQ, Fu LW (2005) J Compos Mater 39:1931
24. Arencon D, Velasco JI (2009) Materials 2:2046
25. Pukánszky B, Vanes M, Maurer FHJ, Vörós G (1994) J Mater Sci 29:2350. doi:10.1007/BF00363426
26. Zhuk AV, Knunyants NN, Oshmyan VG, Topolkaraev VA, Berlin AA (1993) J Mater Sci 28:4595. doi:10.1007/BF00414247
27. Zhang H, Zhong Z, Yang JL, Friedrich K (2006) Polymer 47:679
28. Yu JH, Wang GQ, Chen JF, Zeng XF, Wang WY (2007) Polym Eng Sci 47:201
29. Zhou RJ, Burkhart T (2010) J Thermoplast Compos Mater 23:487
30. Way JL, Atkinson JR, Nutting J (1974) J Mater Sci 9:293. doi:10.1007/BF00550954
31. Friedrich K (1983) Adv Polym Sci 52/53:225
32. Ouederni M, Philips PJ (1996) J Eng Appl Sci 2:2312
33. Razavi-Nouri M, Ghorbanzadeh-Ahangari M, Fereidoon A, Jahanshahi M (2009) Polym Test 28:46